Stem Cell Research & Therapy

RESEARCH

Open Access

The PAR6B-PRKCI-PAR3 complex influences alveolar regeneration in patients with the emphysema subtype of chronic obstructive pulmonary disease

Di Wang[1†], Hongbo Liu[1†], Shuang Bai[1], Xuejian Zheng[1] and Li Zhao[1*]

Abstract

Background Chronic obstructive pulmonary disease (COPD) is gaining increasing attention, with different subtypes being distinguished for separate research and treatment. The emphysema subtype is characterized by widespread alveolar destruction, which may be associated with aggravated alveolar damage and abnormal repair. Type II alveolar epithelial cells (AEC2s), known for their stem cell potential, have recently emerged as a promising target for COPD treatment. However, to date, few studies have elucidated the specific mechanisms by which AEC2s induce alveolar regeneration.

Methods Lung tissue samples from COPD patients were collected, and bioinformatics analysis was used to identify expression profiles affecting the emphysema phenotype and target genes regulating AEC2 proliferation. In vitro models of smoke-induced injury and viral transfection were established to clarify the role of the target gene *PARD6B* in regulating AEC2s proliferation and transdifferentiation potential. Co-immunoprecipitation and mass spectrometry were employed to elucidate the specific regulatory mechanisms. Primary mouse AEC2s were isolated for 3D spheroid formation experiments to further validate the role of the target gene.

Results We observed impaired self-proliferation and enhanced transdifferentiation of AEC2s into AEC1s in lung tissues from COPD patients with emphysema subtype, which was associated with reduced expression of PARD6B. Interestingly, PARD6B primarily functioned as part of a complex in AEC2s. Mechanistically, we found that reduced levels of the PAR3-PARD6B-PRKCI complex could arrest the cell cycle of AEC2s in the G0-G1 phase, thereby impairing their self-proliferation.

Conclusions Our findings reveal a novel regulatory mechanism for alveolar regeneration, highlighting a potential therapeutic target for managing the emphysema subtype of COPD.

Keywords Type II alveolar epithelial cells, Cell proliferation, Alveolar regeneration, Emphysema, Chronic obstructive pulmonary disease

[†]Di Wang and Hongbo Liu contributed equally to this work.

*Correspondence:
Li Zhao
lzhaoli@163.com

[1]Department of Pulmonary and Critical Care Medicine, Shengjing Hospital of China Medical University, Shenyang, China

Background

Chronic Obstructive Pulmonary Disease (COPD) is a progressive lung disease characterized by restricted airflow. With the exacerbation of the global aging population, the medical and social burden caused by COPD is increasing. In 2019 alone, COPD resulted in 3.23 million deaths [1]. Currently, COPD is classified into two subtypes: chronic bronchitis and emphysema. In recent years, as COPD has gained increasing attention, drugs targeting the chronic bronchitis subtype have been developed, such as bronchodilators or anti-inflammatory agents [2, 3]. However, for the emphysema subtype, effective therapeutic strategies for controlling symptoms and preventing deterioration are limited. The emphysema subtype, in addition to airflow restriction, involves the destruction of bronchial walls and alveoli [4], leading to excessive inflation of lung tissues and decreased elasticity. To date, there is still no treatment that can successfully induce lung regeneration in the emphysema subtype.

Recent studies suggest that Type II alveolar epithelial cells (AEC2s), which possess stem cell potential, can proliferate through mitosis to replenish their own numbers after lung injury and differentiate into Type I alveolar epithelial cells (AEC1s) to repair the alveolar epithelial barrier, playing a crucial role in maintaining alveolar epithelial homeostasis [5, 6]. The extensive destruction of alveoli in the emphysema subtype of COPD (ECOPD) is associated with impaired AEC2s which lead to abnormal repair. Therefore, understanding the potential mechanisms that regulate the proliferation, division and differentiation of AEC2s could provide valuable insights into lung regeneration and potentially offer breakthroughs in the treatment of ECOPD.

Symmetric and asymmetric cell division play a crucial role in the dynamic balance and regeneration of tissues [7, 8]. The proliferation and division of AEC2s ensure a balance between self-renewal and differentiation of alveoli, contributing to lung tissue regeneration in the ECOPD. Recent research suggests that the assembly of apical domain structures in epithelial cells can autonomously inhibit the local accumulation of cytoplasmic division components [9], playing a positive role in epithelial cell division [10]. Partitioning defective 6 homolog beta (PARD6B), as a member of the PAR protein family, is closely associated with the apical domain structures in epithelial cells and is widely present in various eukaryotes. It plays a crucial role in the symmetric and asymmetric division of epithelial cells, as well as in maintaining morphology and development [11]. However, the impact of PARD6B on the proliferative division function of AEC2s is currently unclear. Furthermore, research on the caenorhabditis elegans has revealed that PAR6 can form a ternary complex with protein kinase C iota type (PRKCI) and proteinase-activated receptor 3 (PAR3) through its PDZ domain. Abnormal expression of this complex may affect the direction of cell symmetric and asymmetric division and cell fate [12, 13]. In this study, we collected human lung tissue samples to identify potential genes that regulate AEC2s proliferation and transdifferentiation. We further investigated the pathways affecting these genes by extracting primary mouse alveolar epithelial cells and conducting mass spectrometry analysis. These findings may reveal a novel pathway for lung tissue regeneration, which could potentially contribute to advancements in the treatment of ECOPD.

Methods

Subjects and sample preparation

The inclusion criteria for participants were as follows: (1) age between 40 and 80 years; (2) a smoking history of at least 10 pack-years; (3) post-bronchodilator FEV1/FVC < 0.7; (4) evident respiratory symptoms, such as chronic cough with sputum production and/or dyspnea; (5) high-resolution chest computed tomography performed within the last 4 weeks; (6) elective thoracic surgery; (7) signed informed consent. Exclusion criteria for participants were as follows: (1) presence of other respiratory diseases (such as bronchial asthma, bronchiectasis, or active pulmonary tuberculosis) or other chronic and autoimmune diseases; (2) occurrence of infectious diseases within the last 4 weeks (including pulmonary and/or systemic infections).

Lung tissue specimens were obtained from surgically resected lung tissues based on the aforementioned criteria during thoracic surgery. Normal lung tissue was collected from locations as far away from the tumor as possible (linear distance of at least 5 cm), avoiding small airways during collection, and ensuring each lung tissue sample contained an equal amount of lung parenchyma, small airways, and pulmonary blood vessels to ensure sample homogeneity.

Isolation of primary cells and cell culturing

The mouse alveolar epithelial cell line (MLE12 cell line) and primary mouse AEC2s were cultured in DMEM/F12 medium supplemented with 10% fetal bovine serum, 1% penicillin and streptomycin, in a 5% CO_2, 37℃ cell incubator. The MLE12 cell line was purchased from Sunncell Company (SNL-414, Wuhan, China) [14]. Primary mouse AEC2s were extracted using fluorescence-activated cell sorting (FACS). Specifically, the 6-8-week-old C57BL/6 mice were anesthetized by being placed in an anesthesia chamber containing 2.5% isoflurane (RWD, Shenzhen, China) and then were quickly euthanized by cervical dislocation. And their lung tissue was subsequently collected and minced. Then the lung tissue was digested with 0.25% trypsin for 30 min, followed by 0.1% collagenase digestion for 20 min. After centrifugation

at 1000 rpm for 5 min, the cell pellet was resuspended in serum-free DMEM/F12 medium. FITC anti-mouse CD326 antibody (1:200, Biolegend, CA, USA) and APC anti-mouse CD140a antibody (1:40, eBioscience, CA, USA) were used for cell staining, incubated at 4℃ for 30 min. After centrifugation at 800 rpm for 5 min, cells were washed twice with PBS. Finally, cells were resuspended in serum-free DMEM/F12 medium and sorted using FACS Vantage SE. FACS Diva (BD Biosciences, CA, USA) was used for data analysis, and $CD140a^-$ $CD326^+$ cells were identified as AEC2s.

Viral transfection and cell model construction

Prior to transfection, MLE12s and AEC2s were seeded in a 24-well cell culture plate and allowed to reach 30–50% confluence (approximately 1.5×10^5 cells/well). PARD6B overexpression (oePARD6B) lentivirus, PARD6B knockdown (kdPARD6B) lentivirus, and control lentivirus were respectively transfected into cells using polybrene (Hanbio, Shanghai, China). The lentivirus titer was maintained at 4×10^8 TU/ml, and diluted lentivirus was added at an MOI value of 20. Puromycin was used for selecting successfully transfected cells. Cells were further cultured to obtain stable oePARD6B or kdPARD6B cells.

One cigarette (containing 1.2 mg nicotine, 15 mg tar) was completely dissolved in 10 ml of complete medium to obtain a 100% concentration of cigarette smoke extract (CSE). Cells were treated with 6% CSE for 24 h, and then passaged every two days at a 1:3 ratio. The passaged cells were treated with 6% CSE (≥ 3 times) to establish a cell model of chronic cigarette smoke injury. Cells were treated with 0.1mmol/L sodium aurothiomalate (ATM) (Yuanye Bio-Technology, Shanghai, China), an inhibitor of the PB1 domain [15], for 96 h to disrupt the PAR3-PAR6B-PRKCI complex.

qRT-PCR experiments and western blot analysis

RNAiso Plus (TaKaRa, Beijing, China) was used to extract total RNA from each sample. PrimeScript™ RT reagent Kit with gDNA Eraser (TaKaRa, Beijing, China) and TB Green® Premix Ex Taq™ (Tli RNaseH Plus) (TaKaRa, Beijing, China) was used to perform reverse transcription. Primer sequences for each gene are shown in Table S1.

RIPA lysis buffer was used to extract total proteins, and the BCA protein concentration assay kit (Solarbio, Beijing, China) was used to quantifify the concentration of proteins. Equal amounts of denatured proteins were loaded in sodium dodecyl sulfate-polyacrylamide gel electrophoresis and transferred to a polyvinylidene flfluoride membrane. The membrane was blocked with 5% skim milk, and incubated overnight with the primary antibody. The following antibodies were used: anti-GAPDH, anti-PARD6B, anti-PAR3 and anti-PRKCI from Proteintech (IL, United States). Detailed information on antibodies is shown in Table S2. On the following day, the membranes were incubated with secondary antibodies for 1.5 h. The membranes were visualized using enhanced chemiluminescence reagent. ImageJ V1.54 was used for analyzing final images.

Immunohistochemistry and immunofluorescence

Previously embedded patient lung tissue wax blocks were sectioned into paraffin slices. Paraffin slices were deparaffinized sequentially in a series of xylene, anhydrous ethanol, and PBS, followed by heat-induced antigen retrieval in citric acid-sodium citrate buffer. On the other hand, cells intended for observation were prepared as cell smears treated with 4% paraformaldehyde. Both paraffin slices and cell smears were incubated in 10% goat serum at room temperature for 2 h and overnight at 4℃ for primary antibody incubation. In addition to the antibodies used in Western blotting, anti-Sftpc (Surfactant protein C) (Proteintech, IL, USA) and anti-Pdpn (Podoplanin) (Santa Cruz Biotechnology, CA, USA) were also employed. The next day, slices were incubated for 4 h in secondary antibodies. Paraffin slices used for immunohistochemistry underwent DAB staining, followed by uniform tissue staining with hematoxylin for 4 min, rinsing in running water for 30 min. Subsequently, the slices were dehydrated and transparentized in a series of alcohols and xylene, and mounted using neutral gum. Paraffin slices and cell smears for immunofluorescence were counterstained with DAPI for 5 min and mounted using anti-quenching mounting medium. Observation and image acquisition were performed under a microscope.

The hematoxylin and eosin (H&E) staining

The H&E staining was conducted in 2.5-μm thick paraffin slices used above. The slices after deparaffinized were stained for 4 min with hematoxylin (Beyotime, Shanghai, China), rinsed in running tap water for 30s–1 min.Then eosin (Beyotime, Shanghai, China) was used to stain for 2 min to visualize under light microscope.

Immunoprecipitation combined with mass spectrometry analysis

The Dynabead Protein G Immunoprecipitation Kit was used for immunoprecipitation of CSE-treated MLE12 cells. Specifically, total protein was extracted using NP40 lysis buffer. Magnetic beads, primary antibodies, and Ab Binding & Washing Buffer were mixed in a DNA mixer and incubated at room temperature for 10 min. After removal of nonspecific binding with Ab Binding & Washing Buffer, total protein was added and incubated at room temperature for 10 min, ensuring sufficient binding between the primary antibody and the target protein. Washing Buffer was used again to remove nonspecific binding. Elution Buffer and Loading buffer were added,

and the protein mixture was heated at 70℃ for 10 min. The resulting supernatant represented the denatured protein solution. The denatured protein solution underwent vertical electrophoresis, followed by mass spectrometry analysis.

Cell proliferation assay and sphere formation assay

Cell Counting Kit-8 (CCK-8, MCE, NJ, USA) were utilized to assess MLE12 cells proliferation ability. CSE-treated or ATM-treated cells, as well as transfected cells, were seeded onto a 96-well cell culture plate at a density of 2000 cells/well and incubated at 37℃. Subsequently, serum-free medium containing CCK-8 solution was added to each well and incubated for 1 h at 37℃. Finally, absorbance was measured at a wavelength of 450 nm using a spectrophotometer (Bio-Rad, CA, USA).

The sphere formation assay was employed to evaluate AEC2s proliferation and differentiation. Extracted primary AEC2s were resuspended in serum-free DMEM/F12 medium. 250 cells/well were seeded into a 96-well plate and cultured for 7 days. The medium was changed every 2 days. Imaging of five randomly selected regions from each group was performed using a microscope (Leica, Wetzlar, Germany). The sphere percentage was calculated as the number of spheres/250 [16].

Cell cycle analysis

For cell cycle phase analysis, cells were plated in a 6-well plate at a density of 1×10^5 cells/well. After treated with CSE, ATM or transfected with lentivirus, cells were fixed in 70% cold ethanol overnight at − 20℃. The fixed cells were then washed in PBS and incubated with the Cell Cycle Staining Kit (Abbkine, Wuhan, China) in the dark for 30 min at 37℃. The stained cells were subsequently analyzed using a FACScalibur Flow Cytometer (BD, NYC, USA).

Bioinformatics analysis and statistical analysis

Datasets GSE27597, GSE1650, and GSE119040, pertinent to lung tissues of ECOPD, were selected and downloaded from the public Gene Expression Omnibus (GEO) database [17] (see detailed information in Table S3). Differential analysis of gene expression levels in the aforementioned datasets was conducted using GEO2R, and the intersection was taken to identify differentially expressed genes associated with the COPD emphysema phenotype. Pathway and process enrichment analyses were executed using Metascape [18] to identify genes closely related to alveolar regeneration. STRING [19] was used to construct protein interaction network. Continuous variables underwent assessment through the T-test, and categorical variables were appraised using the χ^2 test or Fisher's exact test. Statistical significance was determined by a p-value less than 0.05. Genes exhibiting $|$ fold change $|$ ≥1.5 ($|$ FC $|$ ≥1.5) and $p < 0.05$ were designated as differentially expressed genes (DEGs). The work has been reported in line with the ARRIVE guidelines 2.0.

Result

The proliferation ability of AEC2s is reduced and may be regulated by PARD6B

From April 2017 to September 2021, a total of 26 lung tissue samples were collected from COPD patients undergoing thoracic surgery, including 13 samples from patients with emphysema subtype of COPD (ECOPD) and 13 samples from non-emphysema subtype of COPD (NECOPD). Both groups exhibited no significant differences in gender, age, smoking history, degree of airflow limitation, and pathological tumor type and differentiation. Specific demographic characteristics are presented in Table 1. Immunofluorescence staining was performed on paraffin sections of COPD patient lung tissues. The results revealed the presence of intermediate cells undergoing transition from AEC2s to AEC1s within the damaged lung tissue (indicated by white arrows in Fig. 1a). This suggests that AEC2s possess certain stem cell-like functions, and injured AEC1s are replenished by the proliferation and transdifferentiation of AEC2s. Counting AEC2s, AEC1s, and cells undergoing transdifferentiation from AEC2s to AEC1s, we observed a significant decrease in the proportion of AEC2s and a significant increase in the proportion of cells undergoing transdifferentiation to AEC1s in the ECOPD group compared to the NECOPD group (Fig. 1b). This indicates a diminished regenerative capacity and an enhanced transdifferentiation ability of AEC2s in the emphysema subtype.

Differential analyses were performed on three datasets from the GEO database (GSE1650, GSE27597, and GSE119040). 1493, 840, and 579 DEGs ($p < 0.05$,$|$FC$|$ ≥ 1.5) were found respectively. The intersection of DEGs from the three datasets yielded eight common DEGs exhibiting significant transcriptional differences across all datasets (Fig. 1c). Additionally, functional enrichment analyses were conducted on DEGs from all three datasets. Multiple pathways related to epithelial cell proliferation and differentiation were identified in the enrichment results (Fig. 1d). Notably, among the eight common DEGs, PARD6B was the only gene associated with cell division, proliferation, and differentiation.

Next, we detected the expression level of PARD6B in the lung tissues of COPD patients and the MLE12 cells. The results showed a decreasing trend of *PARD6B* expression at the mRNA level in lung tissues of ECOPD patients, while there was a significant decrease at the protein level ($p < 0.0001$, Fig. 1e). Moreover, in the smoke-induced injury model of MLE12 cells, we observed a significant decrease in Pard6b expression at the protein level ($p < 0.0001$, Fig. 1f). Furthermore, immunohistochemistry

Table 1 Demographic characteristics and lung function indicators of the subjects

	ECOPD (*n*=13)	NECOPD (*n*=13)	*p* Value
Age, years	63.08±7.262	64.15±5.210	0.668
Gender			1.000
Male, n(%)	12(92.3)	12(92.3)	
Female, n(%)	1(7.7)	1(7.7)	
Exposure of injurious agents			1.000
Tobacco history, n(%)	11(84.6)	10(76.9)	
Non-tobacco history, n(%)	2(15.4)	3(23.1)	
Living place			1.000
Living in rural place, n(%)	3(23.1)	2(15.4)	
Living in urban place, n(%)	10(76.9)	11(84.6)	
Pulmonary function test before bronchodilator (ECOPD *n*=13, NECOPD *n*=13)			
FVC	3.400±0.881	3.455±0.908	0.878
FVC%	85.946±18.296	88.892±20.494	0.702
FEV1	2.176±0.771	2.232±0.781	0.857
FEV1%	69.308±22.160	72.908±23.136	0.689
FEV1/FVC%	62.234±8.485	63.283±8.581	0.757
Pulmonary function test after bronchodilator (ECOPD *n*=10, NECOPD *n*=11)			
FVC	3.453±0.663	3.612±0.705	0.601
FVC%	88.390±12.178	94.245±16.370	0.362
FEV1	2.128±0.594	2.226±0.623	0.715
FEV1%	69.420±16.721	74.636±19.275	0.515
FEV1/FVC%	61.213±7.926	61.052±8.777	0.965

was performed to determine the main cell types and subcellular localization of PARD6B expression in lung tissues. The results revealed widespread expression of PARD6B in AEC1s and AEC2s cells, primarily localized to the cell membrane, with minimal expression in the nucleus and cytoplasm. Additionally, the expression of PARD6B was higher in lung tissues of ECOPD patients compared to NECOPD patients (Fig. 1g).

PARD6B promotes the proliferation of AEC2s

Lentivirus was used to knock down and overexpress Pard6b in AEC2s cells. To avoid off-target effects of knockdown RNA, we simultaneously used three different knockdown RNA sequences targeting *Pard6b* and validated the mRNA (Fig. 2a) and protein levels of Pard6b (Fig. 2b). We selected the sequence with the best knockdown efficiency for subsequent experiments. Additionally, we induced cigarette smoke extract (CSE) injury in a 6% CSE-induced smoke injury model and assessed cell proliferation capacity through CCK8 assays. The results showed that knockdown of Pard6b and treatment with CSE reduced the proliferation capacity of cells, while overexpression of Pard6b increased cell proliferation. Moreover, overexpression of Pard6b partially restored the proliferation capacity of cells after knockdown (Fig. 2c).

Furthermore, flow cytometry experiment was performed to detect the distribution of cells in different phases of the cell cycle. We found that the percentage of cells in the G0-G1 phase significantly increased in the CSE-treated group and the Pard6b knockdown group, indicating that knockdown of Pard6b and CSE-induced smoke injury resulted in cells being arrested at the interphase and unable to enter the mitotic phase (Fig. 2d, e). Besides confirming that Pard6b affects the proliferation of the MLE12 cell line, we also evaluated the proliferation capacity of primary mouse AEC2s (pAEC2s, $CD326^+$ $CD140a^-$) (Supplementary Fig. 1). Using lentivirus with the aforementioned sequences, we knocked down Pard6b in pAEC2s and observed the sphere formation ability of pAEC2s in the knockdown group and the control group. The results showed that the sphere-forming abilit was significantly reduced in kdPard6b group (Fig. 2f, g). Interestingly, we found that PARD6B, as an adapter protein, is probably involved in the formation of epithelial tight junctions [20, 21]. To avoid the influence to spheroid data by cell sticking via junctional molecules, immunoprecipitation experiments was conducted targeting RAC1 and CDC42, which can interact with PAR6 through its PDZ domain. We found this interaction is closely linked to tight junction assembly and the polarization of epithelial cells in Drosophila [22, 23]. The result showed that no direct interaction between RAC1, CDC42, and PARD6B (Supplementary Fig. 2).

PARD6B influences the transdifferentiation of AEC2s

The expression levels of AEC2s markers (Sftpc) and AEC1s markers (Pdpn) over time were detected in pAEC2s. The expression levels of Sftpc and Pdpn in

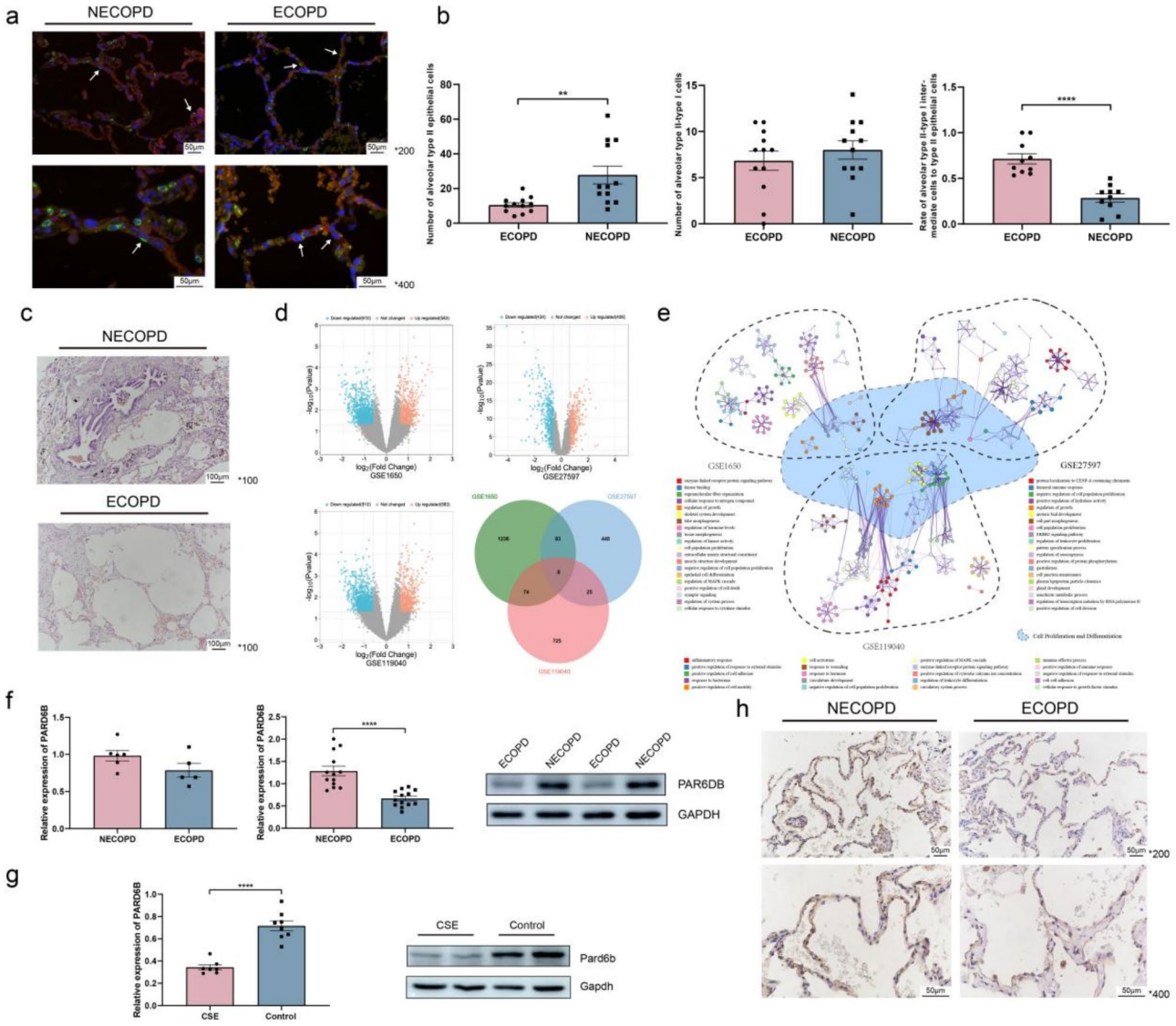

Fig. 1 The proliferation ability of AEC2s is reduced and the transdifferentiation ability is enhanced in emphysema, which may be regulated by PARD6B. **a-b**Immunofluorescence staining of COPD lung tissue. AEC2s are stained green, AEC1s are stained red. Intermediate cells from AEC2s to AEC1s are stained both green and red, which are showed with white arrow. Quantitative results are presented in (**b**). **c** H&E stain of COPD lung tissue. **d** Volcano plot and venn diagram display intersection of DEGs in GEO datasets between emphysema phenotype and non-emphysema phenotype. **e** Functional enrichment analysis of DEGs, revealing functions related to proliferation and differentiation. **f-g** The mRNA and protein levels of PARD6B in lung tissue from COPD patients (**f**) and MLE12 cells (**g**). Full-length blots are presented in Supplementary Fig. 3. **h** The main cell types and subcellular localization of PARD6B in lung tissues with COPD. The values are the mean ± SD. * $p < 0.05$, ** $p < 0.01$, *** $p < 0.001$, **** $p < 0.0001$

pAEC2s after knockdown of Pard6b showed little variation over time (Fig. 3a, c), while the rate of decrease in Sftpc expression and the rate of increase in Pdpn expression over time were slowed down in Pard6b overexpression group compared to that in the control group (Fig. 3b, d). This suggests that Pard6b may have an inhibitory effect on the transdifferentiation ability of AEC2s.

PARD6B forms a complex with PAR3 and PRKCI in AEC2s

Immunoprecipitation of proteins interacting with Pard6b was performed in the CSE-induced smoke injury model. The results showed protein aggregations at 140kd, 75kd, 55kd, 50kd, and 25kd (Fig. 4a). Through mass spectrometry analysis of the obtained proteins, we identified 225 proteins (Table S4) and found four proteins directly associated with Pard6b through PPI network: Llgl1, Llgl2, Prkci, and Par3 (Fig. 4b). Based on literature review and functional enrichment results, we speculated that PAR3 and PRKCI might be binding proteins of PARD6B involved in proliferation functions. Furthermore, we found that PARD6B co-localizes with PAR3 and PRKCI. Most PARD6B proteins binding to PAR3 and PRKCI

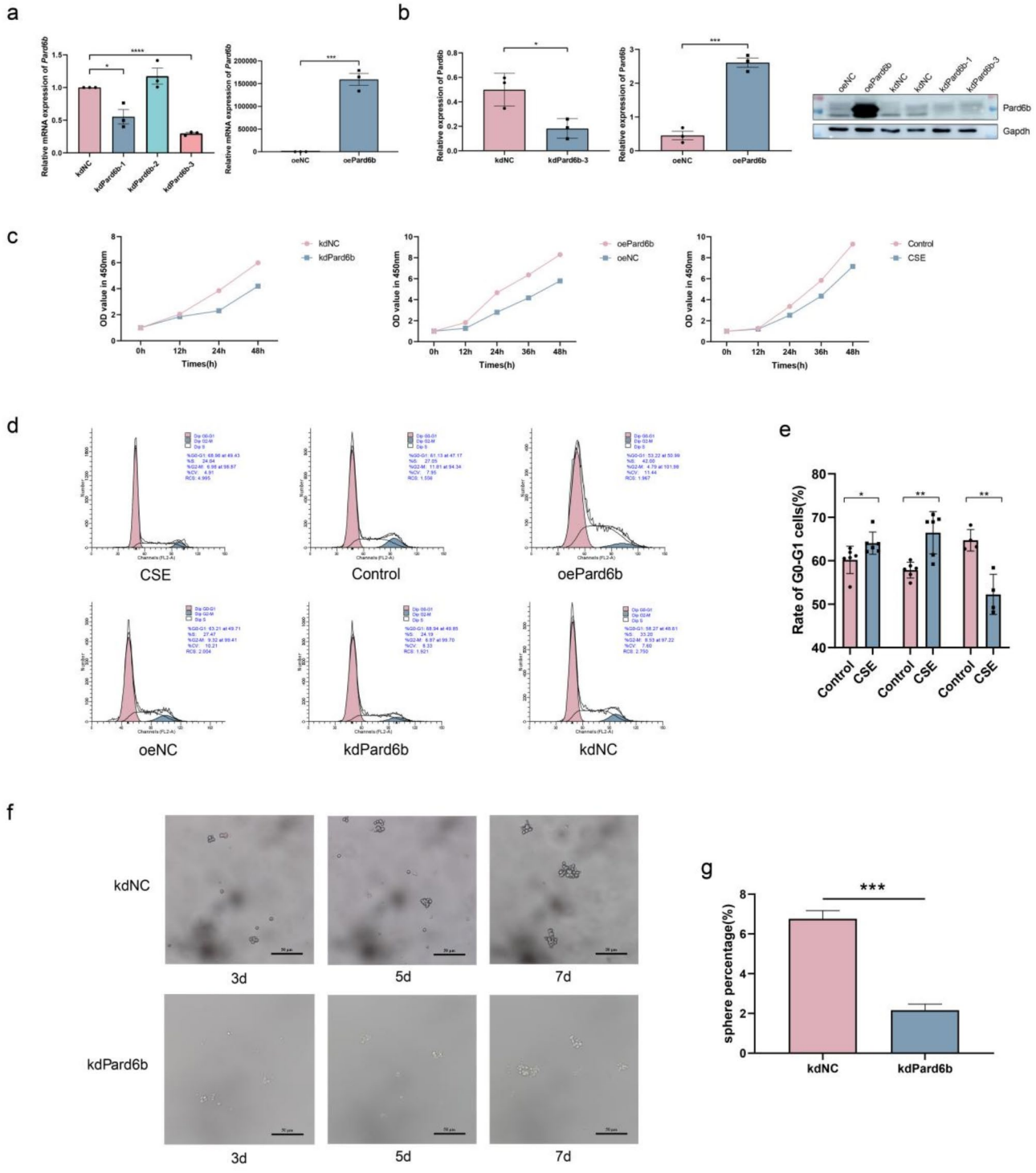

Fig. 2 The proliferation of AEC2s was regulated by PARD6B. **a-b** Validation of Pard6b knockdown and overexpression efficiency in MLE12 cells both at mRNA levels (**a**) and protein levels (**b**). Full-length blots are presented in Supplementary Fig. 4. **c** The proliferation of MLE12 cells can be affected by CSE-induced injury and Pard6b. **d-e** The cell cycle of MLE12 cells can be affected by Pard6b, with quantitative results presented in (**e**). **f-g** The proliferation of pAEC2s can be affected by Pard6b, with quantitative results presented in (**g**)

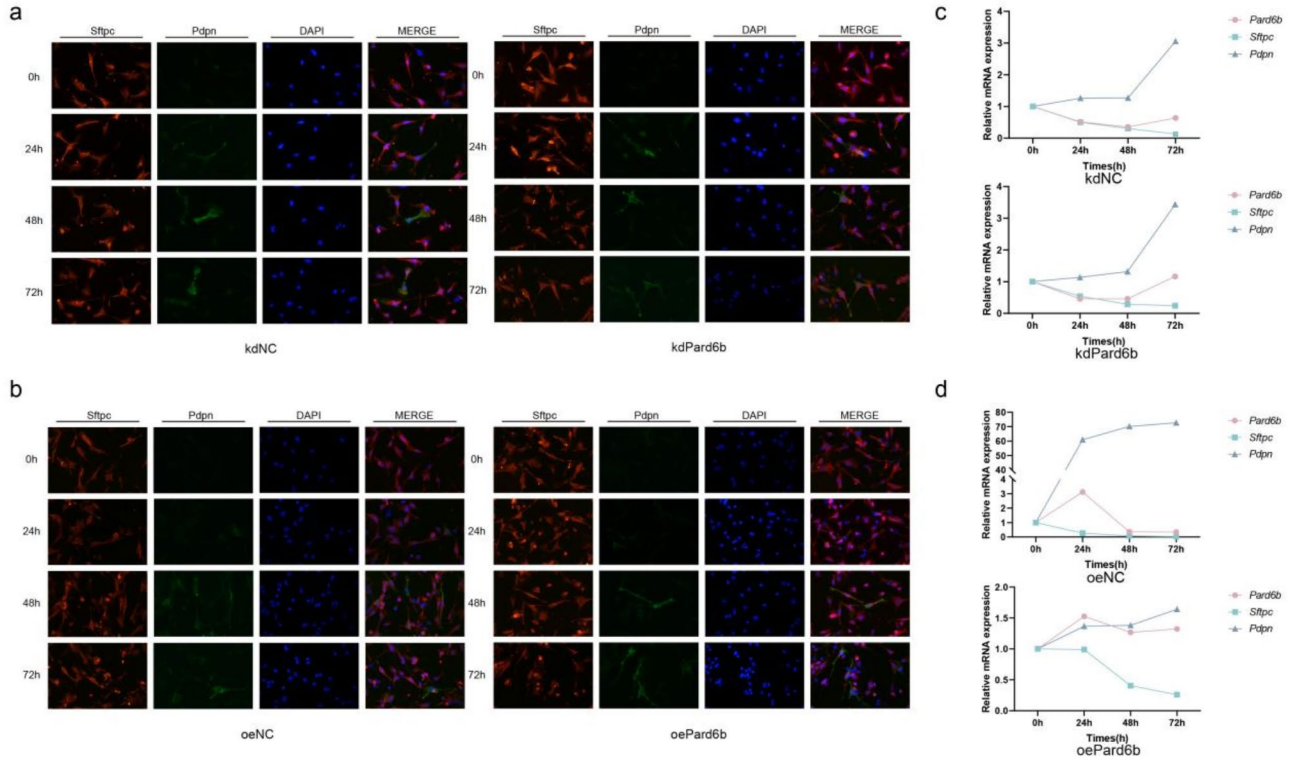

Fig. 3 The transdifferentiation of AEC2s was regulated by PARD6B. **a-b** Immunofluorescence staining of pAEC2s knocking down Pard6b (**a**) and overexpression Pard6b (**b**) at different cell culture time. Green represented Pdpn which was the marker of pAEC1, and red represented Sptfc which was the marker of pAEC2. **c-d** The temporal trends in the mRNA levels of Sptfc and Pdpn in pAEC2s knocking down Pard6b (**c**) and overexpression Pard6b (**d**)

which indicates that the complex is the primary form of PARD6B present in AEC2s. Additionally, the complex level is lower in the ECOPD group compared to the NECOPD group (Fig. 4c-e). Next, we performed immunoprecipitation of proteins interacting with Pard6b in both kdPard6b and oePard6b cell models. The results showed that the expression levels of Par3 and Prkci binding to Pard6b decreased after Pard6b knockdown, while they increased after Pard6b overexpression (Fig. 4f). This demonstrated that the expression level of PARD6B can affect the level of the PAR3-PARD6B-PRKCI complex. Interestingly, we examined the expression levels of single protein in the above complex. The results showed that the expression level of PARD6B significantly decreased in the lung tissues of ECOPD patients and CSE-treated AEC2s ($p < 0.0001$), while the expression levels of PAR3 and PRKCI showed no significant difference (Fig. 4g, h).

The PAR3-PARD6B-PRKCI complex affects the proliferation of AEC2s

We treated MLE12 cells with a compound called ATM, as it has been reported to bind to the PB1 domain on Prkci, thereby inhibiting the binding of Par3, Pard6b, and Prkci [15, 24]. Subsequently, co-immunoprecipitation experiment was performed to verify whether ATM could inhibit the formation of the complex. The results showed that the levels of Par3 and Prkci binding to Pard6b decreased in the ATM-treated group, indicating that ATM could inhibit the formation of the Par3-Pard6b-Prkci complex (Fig. 5a). Furthermore, CCK8 assay was performed to detect cell proliferation ability. The results showed that the proliferation ability of the cells decreased after ATM treatment, and overexpression of Pard6b rescued the proliferation ability of the ATM-treated cells (Fig. 5b, c). Additionally, we assessed the proliferation ability of pAEC2s using the sphere-forming assay. The results indicated that the sphere-forming ability of pAEC2s decreased significantly after ATM treatment (Fig. 5d, e). Moreover, we found that compared to the control group, the percentage of cells in the G0-G1 phase significantly increased in the ATM-treated group (Fig. 5f, g).

Discussion

Our study demonstrates that the formation of the PAR3-PARD6B-PRKCI complex is crucial for the proliferation of alveolar stem cells, namely AEC2s. Although the impact of this complex on drosophila neuroblasts and adult intestinal stem cells has been reported [25, 26], its conserved role in human lung tissue remains understudied. This research is particularly relevant for ECOPD, as the proliferation of AEC2s may promote partial

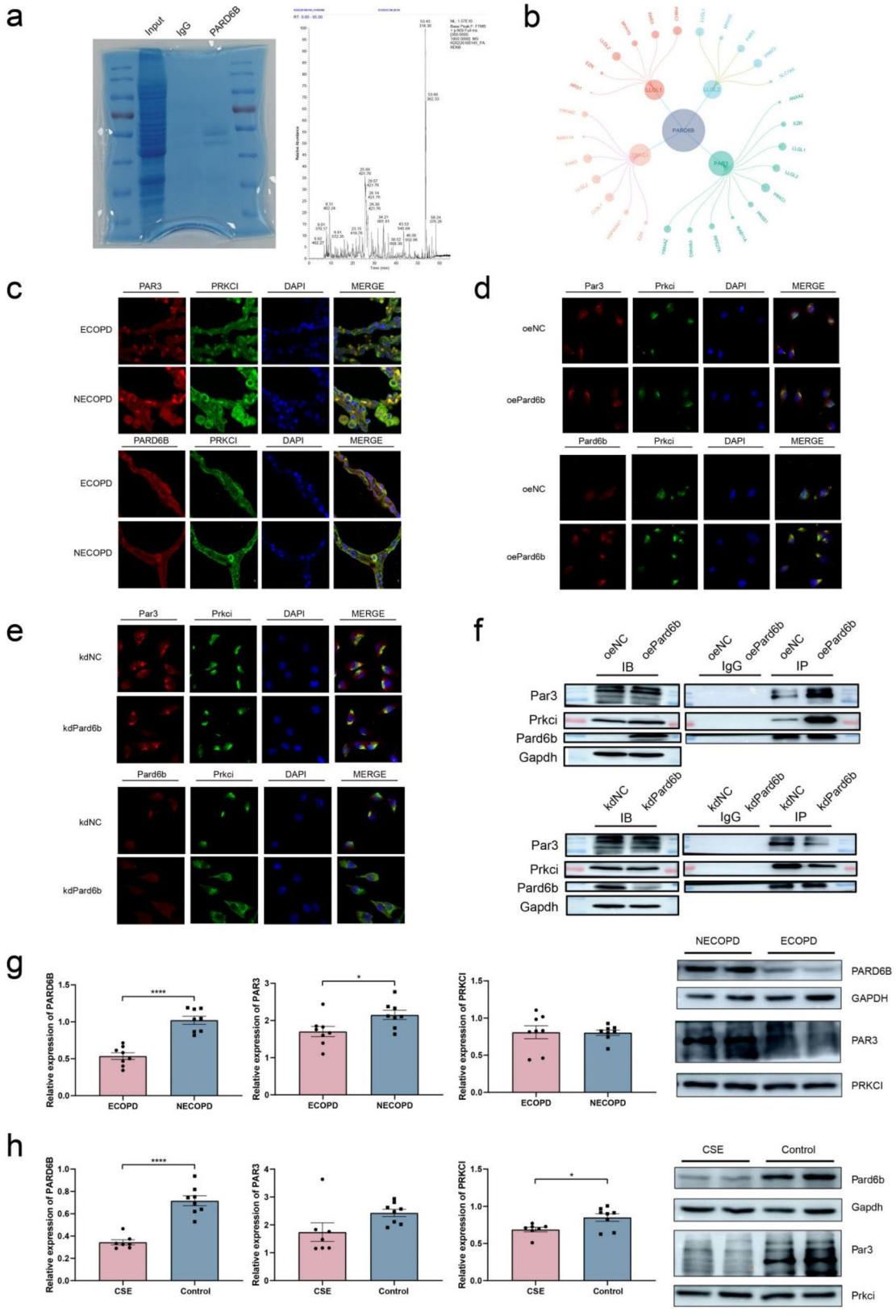

Fig. 4 (See legend on next page.)

(See figure on previous page.)

Fig. 4 PARD6B formed a complex with PAR3 and PRKCI in AEC2s. **a-b**.The results from gel staining and mass spectrometry analysis revealed proteins interacting with Pard6b (**a**) and facilitated the construction of a PPI network map (**b**). **c-e** Immunofluorescence staining of COPD lung tissue (**c**) and MLE12 cells overexpression Pard6b (**d**) and knocking down Pard6b (**e**) revealed PARD6B co-localized with PAR3 and PRKCI. **f** The quantity of the Par3/Pard6b/Prkci complex was affected by the expression level of Pard6b. Input: positive control. IgG: negative control. IP: immunoprecipitation (purified target protein). **g-h** Expression levels of PARD6B, PAR3, and PRKCI in lung tissues of COPD patients (**g**) and MLE12 cells (**h**). Full-length blots are presented in Supplementary Fig. 5

regeneration of lung damage, potentially offering a breakthrough in the treatment of ECOPD patients.

The distal gas exchange region of the lungs is crucial in chronic lung diseases such as COPD or idiopathic pulmonary fibrosis, consisting of millions of alveoli [27]. Each alveolus contains cuboidal AEC2s that express surfactant protein C (SFTPC) and AEC1s, which are thin and adjacent to capillaries. These two cell types have diverse and critical functions. As early as 1969, it was discovered that $SFTPC^+$ AEC2s serve as progenitor cells in alveolar regions of primates and other mammals [28]. Subsequent studies in mice have identified $SFTPC^+$ AEC2s as an epithelial progenitor cell population that generates AEC1s under homeostatic conditions and responds more rapidly to bleomycin-induced lung injury [29]. Furthermore, cell cultures in vitro have shown that AEC2s self-renew and differentiate into intermediate form cells that express both mature AEC2 markers and AEC1 markers, which can form alveolar-like structures (i.e., 'alveolar spheres') in vitro [5]. In this study, we also found similar intermediate form cells in the lung tissues of COPD patients, with a significantly higher proportion of these cells in the emphysema group. This may be due to severe lung tissue damage and AEC2s destruction in the emphysema phenotype, causing the remaining AEC2s to transdifferentiate into AEC1s to compensate for lung damage. This observation is consistent with previous findings in mouse models [29].

In this study, CSE was used to establish the lung injury model. Tobacco smoke is, in fact, one of the most well-established risk factors for emphysema and COPD [30]. Smoking more than 20 packs of cigarettes per year doubles the incidence of COPD in China [31]. During smoking, inflammation, damage, and remodeling are highly activated, and the release of proteases further damages and remodels the lungs through the loss of elastic fibers, leading to the enlargement of alveolar spaces and the development of emphysema [32]. Additionally, other inhaled harmful substances, such as marijuana smoke, can also cause emphysema. In fact, marijuana is the second most commonly smoked substance in society after tobacco. Both substances contain similar harmful and carcinogenic compounds, including phenols, aldehydes, acrolein, benzpyrene, and benzanthracene. Studies show that individuals who smoke marijuana are significantly more likely to experience chronic bronchitis symptoms, such as coughing, sputum production, and wheezing [33]. Furthermore, marijuana and tobacco have cumulative effects in the body. Individuals who smoke both substances are more likely to develop chronic respiratory symptoms than those who smoke only one [34]. In animal models, one study found that mice exposed to marijuana smoke for one week developed severe bronchial hyperreactivity. After one month, they exhibited apical emphysema, and after four months, severe emphysema and bronchial obstruction were observed. Tobacco smoke, in contrast, induced high airway reactivity after two months of exposure in mice but only caused mild emphysema thereafter [35]. This suggests that using marijuana smoke to model emphysema may be a feasible and potentially faster approach. Employing multiple models to explore the pathogenesis of emphysema is meaningful, and this is one of our future research directions.

In fact, most studies on the PAR3-PARD6B-PRKCI complex primarily focus on its role in asymmetric division. Research suggests that this asymmetric division affects the differentiation of AEC2s into AEC1s, which is crucial for lung alveolar repair [36–38]. In our study, we found that in ECOPD patients, there is a simultaneous decrease in the proliferation capacity and an increase in the transdifferentiation capacity of AEC2s. Therefore, we evaluated the effect of PARD6B on both the proliferation and transdifferentiation of AEC2s. Our results showed significant changes in the proliferation capacity of AEC2s after both knocking down and overexpressing PARD6B, whether in primary cells or cell lines. However, only overexpression of PARD6B led to a downward trend in the transdifferentiation capacity of AEC2s, while knocking down PARD6B showed no significant change. This suggests that PARD6B may have some influence on the transdifferentiation capacity of AEC2s, but compared to its effect on proliferation, the evidence for the effect on transdifferentiation is less conclusive. Therefore, we further explored the function of the PAR3-PARD6B-PRKCI complex in the proliferation.

Unlike other studies, we propose that in the lung tissues of ECOPD patients, PARD6B, rather than PAR3 or PRKCI, plays a crucial role in the formation of the PAR3-PARD6B-PRKCI complex. In human lung tissues and the CSE-induced cell injury model, we found a decrease in the expression levels of PARD6B, while the expression levels of PAR3 and PRKCI showed no significant difference. This is probably because PARD6B relies heavily on apical recycling rather than basolateral recycling [39].

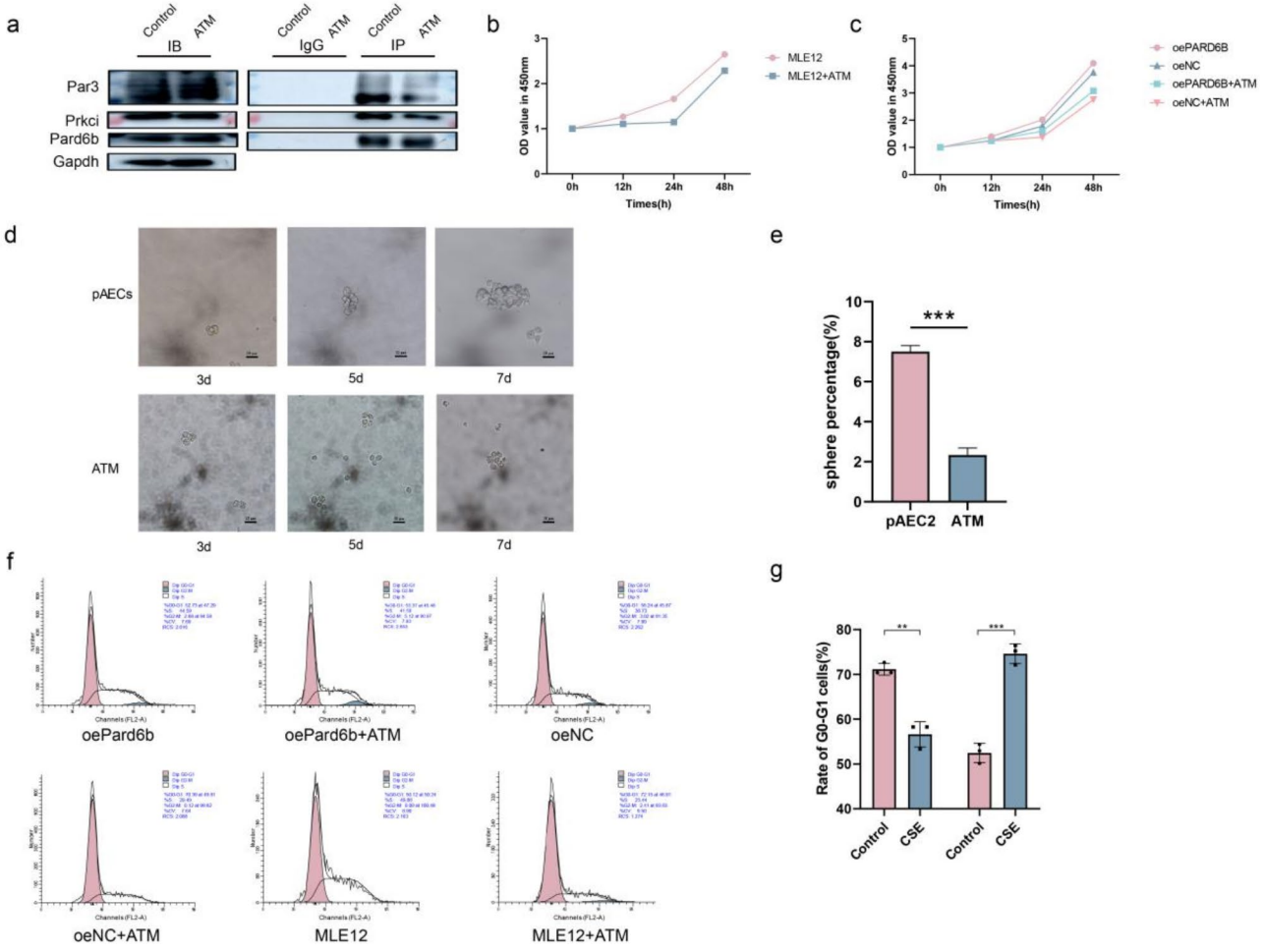

Fig. 5 PAR3-PARD6B-PRKCI complex was involved in regulating the proliferation of AEC2s. **a** The formation of Par3-Pard6b-Prkci complex was inhibited by ATM. Input: positive control. IgG: negative control. IP: immunoprecipitation (purified target protein). Full-length blots are presented in Supplementary Fig. 6. **b-c** The proliferation of AEC2s was affected by the quality of Par3-Pard6b-Prkci complex.The proliferation of MLE12 cells were decreased after ATM treatment (**b**). Overexpression of PARD6B partially rescued the proliferation of MLE12 cells. OD value: absorbance (**c**). **d-e** The sphere-forming ability of pAEC2s decreased significantly after ATM treatment, with quantitative results presented in (**d**). **f-g** The cell cycle of MLE12 cells can be affected by the quality of Par3-Pard6b-Prkci complex, with quantitative results presented in (**g**)

Apical recycling is an important aspect of epithelial cell autonomous host defense. Recent studies have found that certain viruses and bacterial toxins enter epithelial cells through the apical membrane and further infect the host through endocytosis in the apical endosome. The decrease of PARD6B leads to depletion of apical endosome function, making epithelial cells more resistant to further infection from the surface [40]. This may explain why ECOPD patients are more susceptible to viral infections and more prone to acute exacerbations.

Regarding the stability of the PAR3-PARD6B-PRKCI complex in lung tissue, we observed expression of PAR3, PARD6B, and PRKCI in AEC2s on human lung tissue slices, with clear co-localization. However, results from cell immunofluorescence staining suggested that while PARD6B and PRKCI showed good co-localization, PAR3 expression in the cytoplasm appeared more diffuse, and some PAR3 punctate fluorescence signals did not co-localize with PARD6B and PRKCI. This may be due to increasing evidence indicating the dynamic nature of PAR3-PARD6B-PRKCI complex formation [41, 42]. In fact, PARD6 initially forms a stable complex with PRKCI. And PAR3 mainly interacts with the PRKCI-PARD6 complex through PRKCI, inducing the formation of the tripartite complex [21, 43]. Some studies suggest that Rho kinase can disrupt the interaction between PAR3 and the PRKCI-PARD6 complex by phosphorylating PAR3 at Thr883, thereby inhibiting complex formation [44]. Hence, the interaction between PAR3 and PRKCI may be one of the main targets for regulating the activity and localization of the PAR3-PARD6B-PRKCI complex, further explaining why PAR3 and PRKCI-PARD6 complexes do not always co-localize in AEC2s.

Furthermore, to confirm the impact of the PAR3-PARD6B-PRKCI complex on AEC2s cell division and proliferation, we treated the cells with sodium aurothiomalate (ATM). ATM, known for its anti-inflammatory effects, can reduce serum immunoglobulin levels and was used clinically to alleviate symptoms of rheumatoid arthritis. Studies have shown that ATM induces a dose-dependent loss of the PB1 domain [35], the connecting structure between PRKCI and the downstream effector PARD6. Our experimental results confirmed this finding. We found that after treatment with ATM, the proliferation ability of AEC2s decreased. Interestingly, we also found that overexpression of PARD6B partially restored the decreased the proliferation induced by ATM. We beleive that this may be because the binding of ATM to the PB1 domain competitively inhibits the binding between PARD6B and PRKCI. When the concentration of ATM is high, PRKCI cannot bind to PARD6B to form the complex, leading to a decrease in the proliferation of AEC2s. However, when the expression of PARD6B is increased, its competitive binding with PRKCI increases, resulting in an increase in the complex. And the proliferation of AEC2s restored, which is consistent with the findings of Melody et al. [45]. As reported in the study by Melody et al., ATG, an ATM-related compound, was found to block PRKCI-dependent signaling and inhibit the transformed growth of lung cancer cells.

To further elucidate at which stage the PAR3-PARD6B-PRKCI complex specifically affects the proliferation of AEC2s, we conducted cell cycle experiments. We found that after ATM treatment or PARD6B knockdown, the cell cycle was arrested at the G0-G1 phase, preventing entry into the division phase. Investigating the cause of this cell cycle arrest is intriguing. Recent studies have suggested that the PAR3-PARD6B-PRKCI complex can control the orientation of the mitotic spindle in polarized epithelial cells [46] and promote the formation of non-centrosomal microtubules [47]. These mechanisms could potentially inhibit the proliferation of AEC2s, leading to cell cycle arrest.

Despite the substantial evidence obtained from human tissue and cell studies, this research still has limitations. Firstly, there is currently no in vivo validation regarding the regulation of the PAR3-PARD6B-PRKCI complex on the proliferation of AEC2s. Next, we plan to further construct transgenic mice to verify the complex's in vivo effects and its specific regulatory mechanisms on centrosomes, spindle bodies, and nucleoli. Additionally, the cell model induced by CSE does not completely mimic the emphysema phenotype of COPD, although it has been widely used in many studies [48, 49]. There is no standard confirmation because the diagnosis criteria for emphysema phenotype are based on tissue damage rather than cellular changes. However, CSE-induced cell damage partially represents the cellular state in the emphysema phenotype. We will explore better modeling methods to more accurately reproduce the cellular state of the emphysema phenotype.

Conclusion

In summary, we have provided compelling evidence demonstrating that the PAR3-PARD6B-PRKCI complex affects the cell cycle progression, thereby regulating the division and proliferation of AEC2s. This may represent a novel pathway for lung regeneration, ushering in new breakthroughs in the treatment of ECOPD.

Abbreviations

COPD	Chronic obstructive pulmonary disease
AEC2s	Type II alveolar epithelial cells
AEC1s	Type I alveolar epithelial cells
ECOPD	Emphysema subtype of chronic obstructive pulmonary disease
NECOPD	Non-emphysema subtype of chronic obstructive pulmonary disease
PARD6B	Partitioning defective 6 homolog beta
PAR3	Proteinase-activated receptor 3
PRKCI	Protein kinase C iota type
FACS	Fluorescence-activated cell sorting
rpm	Revolutions per minute
CSE	Cigarette smoke extract
ATM	Sodium aurothiomalate
GEO	Gene Expression Omnibus
FC	Fold change
DEGs	Differentially expressed genes
Sftpc	Surfactant protein C
Pdpn	Podoplanin

Supplementary Information

The online version contains supplementary material available at https://doi.org/10.1186/s13287-025-04189-6 .

Supplementary Material 1

Supplementary Material 2

Supplementary Material 3

Supplementary Material 4

Supplementary Material 5

Supplementary Material 6

Supplementary Material 7

Acknowledgements

We sincerely thank all the patients who graciously provided their clinical samples for this study. The authors declare that they have not used AI-generated work in this manuscript.

Author contributions

DW conducted the experiments, wrote the manuscript, and analyzed the data. HL identified clinical diseases, collected samples and analyzed the data. SB collected data and performed experiments. XZ collected samples. LZ supervised the overall progress of the research, revised the manuscript, and acquired fundings. All authors read and approved the final manuscript.

Funding

This work was supported by the following financial sources: National Natural Science Foundation of China (No. 82170047); National Natural Science Foundation of China Young Scientists Fund (No. 82300058).

Data availability
All data generated or analysed during this study are included in this published article and its supplementary information files.

Declarations

Ethics approval and consent to participate
The study was approved by the Ethics Committee of the Shengjing Hospital of China Medical University.
For human samples:
Project: Research on the Mechanisms of the Emphysema Phenotype in Chronic Obstructive Pulmonary Disease. No.2018PS433K. 13th July 2018.
For animal experiments:
Project: Research on the Mechanisms of the Emphysema Phenotype in Chronic Obstructive Pulmonary Disease. No.2018PS410K. 15th June 2018.

Consent for publication
Not applicable.

Competing interests
The authors declare that they have no competing interests.

Received: 7 November 2024 / Accepted: 24 January 2025
Published online: 25 February 2025

References

1. Chronic obstructive pulmonary disease (COPD). https://www.who.int/news-room/fact-sheets/detail/chronic-obstructive-pulmonary-disease-(copd). Accessed 16 May 2023.
2. Andelid K, Ost K, Andersson A, Mohamed E, Jevnikar Z, Vanfleteren L, et al. Lung macrophages drive mucus production and steroid-resistant inflammation in chronic bronchitis. Respir Res. 2021;22:172. https://doi.org/10.1186/s12931-021-01762-4.
3. Staykova T, Black PN, Chacko EE, Poole P. Prophylactic antibiotic therapy for chronic bronchitis. Cochrane Database Syst Rev. 2003;1:CD004105. https://doi.org/10.1002/14651858.CD004105.
4. Tuder RM. Bringing light to Chronic Obstructive Pulmonary Disease Pathogenesis and Resilience. Ann Am Thorac Soc. 2018;15:S227–33. https://doi.org/10.1513/AnnalsATS.201808-583MG.
5. Barkauskas CE, Cronce MJ, Rackley CR, Bowie EJ, Keene DR, Stripp BR, et al. Type 2 alveolar cells are stem cells in adult lung. J Clin Invest. 2013;123:3025–36. https://doi.org/10.1172/JCI68782.
6. Kosmider B, Mason RJ, Bahmed K. Isolation and characterization of human alveolar type II cells. Methods Mol Biol. 2018;1809:83–90. https://doi.org/10.1007/978-1-4939-8570-8_7.
7. Castanon I, Gonzalez-Gaitan M. Oriented cell division in vertebrate embryogenesis. Curr Opin Cell Biol. 2011;23:697–704. https://doi.org/10.1016/j.ceb.2011.09.009.
8. Scepanovic G, Fernandez-Gonzalez R. Oriented cell division: the pull of the Pole. Dev Cell. 2018;47:686–7. https://doi.org/10.1016/j.devcel.2018.11.040.
9. Paim LMG, FitzHarris G. Cell size and polarization determine cytokinesis furrow ingression dynamics in mouse embryos. Proc Natl Acad Sci U S A. 2022;119:e2119381119. https://doi.org/10.1073/pnas.2119381119.
10. Jordan SN, Davies T, Zhuravlev Y, Dumont J, Shirasu-Hiza M, Canman JC. Cortical PAR polarity proteins promote robust cytokinesis during asymmetric cell division. J Cell Biol. 2016;212:39–49. https://doi.org/10.1083/jcb.201510063.
11. Doe CQ. Cell polarity: the PARty expands. Nat Cell Biol. 2001;3:E7–9. https://doi.org/10.1038/35050684.
12. Etienne-Manneville S, Hall A. Cell polarity: Par6, aPKC and cytoskeletal crosstalk. Curr Opin Cell Biol. 2003;15:67–72. https://doi.org/10.1016/s0955-0674(02)00005-4.
13. Pushpa K, Dagar S, Kumar H, Pathak D, Mylavarapu SVS. The exocyst complex regulates C. Elegans germline stem cell proliferation by controlling membrane notch levels. Development. 2021;148. https://doi.org/10.1242/dev.196345.
14. MLE12 (the mouse alveolar epithelial cell line). https://www.sunncell.com.cn/product/SNL-414. Accessed 19 January 2025.
15. Erdogan E, Lamark T, Stallings-Mann M, Lee J, Pellecchia M, Thompson EA, et al. Aurothiomalate inhibits transformed growth by targeting the PB1 domain of protein kinase ciota. J Biol Chem. 2006;281:28450–9. https://doi.org/10.1074/jbc.M606054200.
16. Chen J, Chen T, Zhu Y, Li Y, Zhang Y, Wang Y, et al. circPTN sponges miR-145-5p/miR-330-5p to promote proliferation and stemness in glioma. J Exp Clin Cancer Res. 2019;38:398. https://doi.org/10.1186/s13046-019-1376-8.
17. The Gene Expression Omnibus Database. http://www.ncbi.nlm.nih.gov/geo. Accessed 15 October 2024.
18. Zhou Y, Zhou B, Pache L, Chang M, Khodabakhshi AH, Tanaseichuk O, et al. Metascape provides a biologist-oriented resource for the analysis of systems-level datasets. Nat Commun. 2019;10:1523. https://doi.org/10.1038/s41467-019-09234-6.
19. Szklarczyk D, Kirsch R, Koutrouli M, Nastou K, Mehryary F, Hachilif R, et al. The STRING database in 2023: protein-protein association networks and functional enrichment analyses for any sequenced genome of interest. Nucleic Acids Res. 2023;51:D638–46. https://doi.org/10.1093/nar/gkac1000.
20. Hurd TW, Gao L, Roh MH, Macara IG, Margolis B. Direct interaction of two polarity complexes implicated in epithelial tight junction assembly. Nat Cell Biol. 2003;5:137–42. https://doi.org/10.1038/ncb923.
21. Suzuki A, Yamanaka T, Hirose T, Manabe N, Mizuno K, Shimizu M, et al. Atypical protein kinase C is involved in the evolutionarily conserved par protein complex and plays a critical role in establishing epithelia-specific junctional structures. J Cell Biol. 2001;152:1183–96. https://doi.org/10.1083/jcb.152.6.1183.
22. Petronczki M, Knoblich JA. DmPAR-6 directs epithelial polarity and asymmetric cell division of neuroblasts in Drosophila. Nat Cell Biol. 2001;3:43–9. https://doi.org/10.1038/35050550.
23. Wodarz A, Ramrath A, Grimm A, Knust E. Drosophila atypical protein kinase C associates with Bazooka and controls polarity of epithelia and neuroblasts. J Cell Biol. 2000;150:1361–74. https://doi.org/10.1083/jcb.150.6.1361.
24. Forteza R, Wald FA, Mashukova A, Kozhekbaeva Z, Salas PJ. Par-complex aPKC and Par3 cross-talk with innate immunity NF-kappaB pathway in epithelial cells. Biol Open. 2013;2:1264–9. https://doi.org/10.1242/bio.20135918.
25. Goulas S, Conder R, Knoblich JA. The Par complex and integrins direct asymmetric cell division in adult intestinal stem cells. Cell Stem Cell. 2012;11:529–40. https://doi.org/10.1016/j.stem.2012.06.017.
26. Hapak SM, Rothlin CV, Ghosh S. PAR3-PAR6-atypical PKC polarity complex proteins in neuronal polarization. Cell Mol Life Sci. 2018;75:2735–61. https://doi.org/10.1007/s00018-018-2828-6.
27. Vasilescu DM, Gao Z, Saha PK, Yin L, Wang G, Haefeli-Bleuer B, et al. Assessment of morphometry of pulmonary acini in mouse lungs by nondestructive imaging using multiscale microcomputed tomography. Proc Natl Acad Sci U S A. 2012;109:17105–10. https://doi.org/10.1073/pnas.1215112109.
28. Kapanci Y, Weibel ER, Kaplan HP, Robinson FR. Pathogenesis and reversibility of the pulmonary lesions of oxygen toxicity in monkeys. II. Ultrastructural and morphometric studies. Lab Invest. 1969;20:101–18.
29. Rock JR, Barkauskas CE, Cronce MJ, Xue Y, Harris JR, Liang J, et al. Multiple stromal populations contribute to pulmonary fibrosis without evidence for epithelial to mesenchymal transition. Proc Natl Acad Sci U S A. 2011;108:E1475–83. https://doi.org/10.1073/pnas.1117988108.
30. Vestbo J, Hurd SS, Agusti AG, Jones PW, Vogelmeier C, Anzueto A, et al. Global strategy for the diagnosis, management, and prevention of chronic obstructive pulmonary disease: GOLD executive summary. Am J Respir Crit Care Med. 2013;187:347–65. https://doi.org/10.1164/rccm.201204-0596PP.
31. Wang C, Xu J, Yang L, Xu Y, Zhang X, Bai C, et al. Prevalence and risk factors of chronic obstructive pulmonary disease in China (the China Pulmonary Health [CPH] study): a national cross-sectional study. Lancet. 2018;391:1706–17. https://doi.org/10.1016/S0140-6736(18)30841-9.
32. Upadhyay P, Wu CW, Pham A, Zeki AA, Royer CM, Kodavanti UP, et al. Animal models and mechanisms of tobacco smoke-induced chronic obstructive pulmonary disease (COPD). J Toxicol Environ Health B Crit Rev. 2023;26:275–305. https://doi.org/10.1080/10937404.2023.2208886.
33. Tashkin DP, Marijuana, Disease L. Chest. 2018;154:653–63. https://doi.org/10.1016/j.chest.2018.05.005.
34. Tan WC, Lo C, Jong A, Xing L, Fitzgerald MJ, Vollmer WM, et al. Marijuana and chronic obstructive lung disease: a population-based study. CMAJ. 2009;180:814–20. https://doi.org/10.1503/cmaj.081040.
35. Helyes Z, Kemeny A, Cseko K, Szoke E, Elekes K, Mester M, et al. Marijuana smoke induces severe pulmonary hyperresponsiveness, inflammation, and emphysema in a predictive mouse model not via CB1 receptor activation. Am J Physiol Lung Cell Mol Physiol. 2017;313:L267–77. https://doi.org/10.1152/ajplung.00354.2016.

36. Finn J, Sottoriva K, Pajcini KV, Kitajewski JK, Chen C, Zhang W, et al. Dlk1-Mediated temporal regulation of Notch Signaling is required for differentiation of alveolar type II to type I cells during repair. Cell Rep. 2019;26:2942–e545. https://doi.org/10.1016/j.celrep.2019.02.046.
37. Chen J, Wu H, Yu Y, Tang N. Pulmonary alveolar regeneration in adult COVID-19 patients. Cell Res. 2020;30:708–10. https://doi.org/10.1038/s41422-020-0369-7.
38. Strunz M, Simon LM, Ansari M, Kathiriya JJ, Angelidis I, Mayr CH, et al. Alveolar regeneration through a Krt8 + transitional stem cell state that persists in human lung fibrosis. Nat Commun. 2020;11:3559. https://doi.org/10.1038/s41467-020-17358-3.
39. Nelms B, Dalomba NF, Lencer W. A targeted RNAi screen identifies factors affecting diverse stages of receptor-mediated transcytosis. J Cell Biol. 2017;216:511–25. https://doi.org/10.1083/jcb.201609035.
40. Maeda K, Zachos NC, Orzalli MH, Schmieder SS, Chang D, Bugda Gwilt K, et al. Depletion of the apical endosome in response to viruses and bacterial toxins provides cell-autonomous host defense at mucosal surfaces. Cell Host Microbe. 2022;30:216–e315. https://doi.org/10.1016/j.chom.2021.12.011.
41. Hutterer A, Betschinger J, Petronczki M, Knoblich JA. Sequential roles of Cdc42, Par-6, aPKC, and Lgl in the establishment of epithelial polarity during Drosophila embryogenesis. Dev Cell. 2004;6:845–54. https://doi.org/10.1016/j.devcel.2004.05.003.
42. Nagai-Tamai Y, Mizuno K, Hirose T, Suzuki A, Ohno S. Regulated protein-protein interaction between aPKC and PAR-3 plays an essential role in the polarization of epithelial cells. Genes Cells. 2002;7:1161–71. https://doi.org/10.1046/j.1365-2443.2002.00590.x.
43. Yamanaka T, Horikoshi Y, Suzuki A, Sugiyama Y, Kitamura K, Maniwa R, et al. PAR-6 regulates aPKC activity in a novel way and mediates cell-cell contact-induced formation of the epithelial junctional complex. Genes Cells. 2001;6:721–31. https://doi.org/10.1046/j.1365-2443.2001.00453.x.
44. Nakayama M, Goto TM, Sugimoto M, Nishimura T, Shinagawa T, Ohno S, et al. Rho-kinase phosphorylates PAR-3 and disrupts PAR complex formation. Dev Cell. 2008;14:205–15. https://doi.org/10.1016/j.devcel.2007.11.021.
45. Stallings-Mann M, Jamieson L, Regala RP, Weems C, Murray NR, Fields AP. A novel small-molecule inhibitor of protein kinase ciota blocks transformed growth of non-small-cell lung cancer cells. Cancer Res. 2006;66:1767–74. https://doi.org/10.1158/0008-5472.CAN-05-3405.
46. Durgan J, Kaji N, Jin D, Hall A. Par6B and atypical PKC regulate mitotic spindle orientation during epithelial morphogenesis. J Biol Chem. 2011;286:12461–74. https://doi.org/10.1074/jbc.M110.174235.
47. Castiglioni VG, Pires HR, Rosas Bertolini R, Riga A, Kerver J, Boxem M, Epidermal. PAR-6 and PKC-3 are essential for larval development of C. Elegans and organize non-centrosomal microtubules. Elife. 2020;9. https://doi.org/10.7554/eLife.62067.
48. Aghapour M, Raee P, Moghaddam SJ, Hiemstra PS, Heijink IH. Airway Epithelial Barrier Dysfunction in Chronic Obstructive Pulmonary Disease: role of cigarette smoke exposure. Am J Respir Cell Mol Biol. 2018;58:157–69. https://doi.org/10.1165/rcmb.2017-0200TR.
49. Vij N, Chandramani-Shivalingappa P, Van Westphal C, Hole R, Bodas M. Cigarette smoke-induced autophagy impairment accelerates lung aging, COPD-emphysema exacerbations and pathogenesis. Am J Physiol Cell Physiol. 2018;314:C73–87. https://doi.org/10.1152/ajpcell.00110.2016.

Publisher's note